Nanoscale Res Lett (2010) 5:576–580
DOI 10.1007/s11671-009-9507-3

NANO EXPRESS

Optical Properties of GaAs Quantum Dots Fabricated by Filling of Self-Assembled Nanoholes

Ch. Heyn · A. Stemmann · T. Köppen · Ch. Strelow · T. Kipp · M. Grave · S. Mendach · W. Hansen

Received: 4 November 2009 / Accepted: 9 December 2009 / Published online: 25 December 2009

Abstract Experimental results of the local droplet etching technique for the self-assembled formation of nanoholes and quantum rings on semiconductor surfaces are discussed. Dependent on the sample design and the process parameters, filling of nanoholes in AlGaAs generates strain-free GaAs quantum dots with either broadband optical emission or sharp photoluminescence (PL) lines. Broadband emission is found for samples with completely filled flat holes, which have a very broad depth distribution. On the other hand, partly filling of deep holes yield highly uniform quantum dots with very sharp PL lines.

Keywords Quantum dots · Molecular beam epitaxy · Droplet etching · Photoluminescence · Atomic force microscopy

Introduction

Crystalline semiconductor quantum dots (QDs) can be regarded as artificial atomic-like entities, which intrigue from a fundamental point of view [1]. But semiconductor QDs are also very attractive for device applications where QDs turned out to be superior to bulk material. This has been demonstrated for instance by the first QD-based laser that exhibits a lower threshold current density compared to QW lasers [2]. Further advanced applications for QDs are proposed, such as qubits in quantum computing [3] or single-photon sources in quantum cryptography [4, 5].

Quantum dot fabrication techniques that are based on self-assembling mechanisms during epitaxial growth allow the integration of QD layers into semiconductor heterostructures. In this field, a very prominent example is strain-induced InAs QDs grown on GaAs in the Stranski–Krastanov mode [6–9]. A further interesting method for self-assembled QD generation is the droplet epitaxy in Volmer–Weber mode. The method was first demonstrated by Koguchi and Ishige [10] in 1993. In comparison with the Stranski–Krastanov technique, droplet epitaxy is more flexible regarding the choice of the QD material. For instance, the fabrication of strain-free GaAs QDs [11–13], InGaAs QDs with controlled In content [14, 15], and InAs QDs [16] has been demonstrated.

During droplet epitaxial QD fabrication [17], first liquid metallic droplets are generated on semiconductor surfaces, e.g., by Ga deposition without As flux. The growth temperature $T = 100$–$350°$ typically is kept very low compared to usual MBE growth conditions. After Ga droplet formation, an As pressure is applied in order to crystallize the droplets and transform them into GaAs QDs. Interestingly, deposition of Ga droplets on GaAs at significantly higher temperatures $T = 450$–$620°$ results in the formation of deep nanoholes in the substrate surface. This effect was first observed by Wang et al. [18] in 2007 and represents a local removal of material from semiconductor surfaces without the need of any lithographic steps. As an important advantage compared to conventional lithography processes, this local droplet etching (LDE) is fully compatible with usual MBE equipment and can be easily integrated into the MBE growth of heterostructure devices. LDE was demonstrated in addition on AlGaAs [19, 20] and AlAs [21] surfaces

Ch. Heyn (✉) · A. Stemmann · T. Köppen · Ch. Strelow · T. Kipp · M. Grave · S. Mendach · W. Hansen
Institut für Angewandte Physik und Zentrum für Mikrostrukturforschung, Jungiusstraße 11, 20355 Hamburg, Germany
e-mail: heyn@physnet.uni-hamburg.de

as well as etching with InGa [19, 22–24] and Al [21] droplets.

After droplet etching, the nanohole openings are surrounded by walls that are crystallized from droplet material and may act as quantum rings [19, 22–25]. The crystallization of the walls [26] and the time evolution of the transformation from the initial droplets into nanoholes with wall [27] were studied in previous publications. A first functionalization of the nanoholes, the fabrication of a novel type of very uniform, strain-free GaAs QDs by filling of LDE nanoholes in AlGaAs with GaAs, has been demonstrated [21]. In the present paper we describe the influence of the LDE process and sample design on the optical properties of such GaAs QDs.

Local Droplet Etching and Nanohole Filling

We fabricate LDE nanoholes using solid-source molecular beam epitaxy (MBE) on (001) GaAs wafers. Two different sample designs will be discussed in the following, denoted as type I and type II. After growth of a GaAs buffer layer, a 200-nm-thick $Al_{0.36}Ga_{0.64}$ As barrier layer was deposited. For the samples of type II, an additional 5-nm-thick AlAs layer was grown before LDE. Type I samples have no such AlAs layer. Afterward, the As shutter and valve were closed and droplet formation was initiated at a temperature T_1 by opening the Al shutter for a time $t_1 = 6$ s. We used Al droplets for etching in order to avoid an additional carrier confinement by the wall. The temperatures were $T_1 = 620°$ for the type I samples and $T_1 = 650°$ for the type II samples with the additional AlAs layer. During this stage, a strongly reduced arsenic flux is important [26]. The As flux in our experiments was approximately hundred times lower compared to typical GaAs growth conditions. The Al flux F corresponded to a growth speed of 0.47 ML/s, and droplet material was deposited onto the surface with coverage $\theta = F\ t_1$. After droplet deposition, the temperature was set to a value T_2, and a thermal annealing step of time t_2 was applied in order to remove liquid etching residues. For the present samples, we have used $T_2 = T_1$ and $t_2 = 180$ s.

A sketch of the different stages during LDE is shown in Fig. 1. The key process for nanohole creation is the diffusion of As from the substrate into the droplet, which causes the liquefaction of the substrate below the droplet. From the measured hole volume, we have estimated a value of 0.03 ± 0.01 for the average As concentration in the droplet material [26]. The formation of the walls surrounding the nanohole openings is explained by the assumption that As diffuses to the droplet surface and crystallizes during the annealing step with droplet material at the interface to the substrate [19, 26]. Furthermore, coarsening by Ostwald ripening [28] reduces the droplet density before drilling and a delay of both, the hole drilling process, as well as the removal of the liquid material after etching was detected [27].

Figure 2a shows an atomic force microscopy (AFM) image of an AlGaAs surface after local droplet etching with Al and Fig. 2b the corresponding hole depth distribution. Clearly visible is a bimodal depth distribution with deep (Fig. 2d) and shallow (Fig. 2c) nanoholes in agreement with previous results [20] for Ga LDE. Typical deep holes have an average depth of $d_H = 14$ nm, and slightly elliptical openings with axis of 39 nm along [1–11] direction and 33 nm along [110]. The surface shown in Fig. 2a is exemplary for type I samples and was used for the fabrication of QDs with broadband light emission. From earlier results, [20] we know that the formation of flat nanoholes can be suppressed by performing the LDE

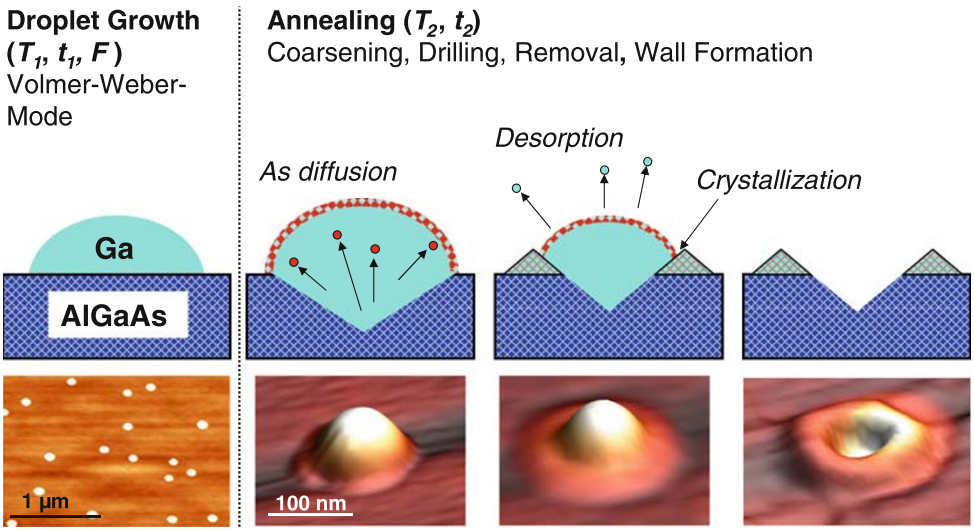

Fig. 1 Sketch of the different stages during LDE resulting in nanohole and wall formation together with corresponding AFM images

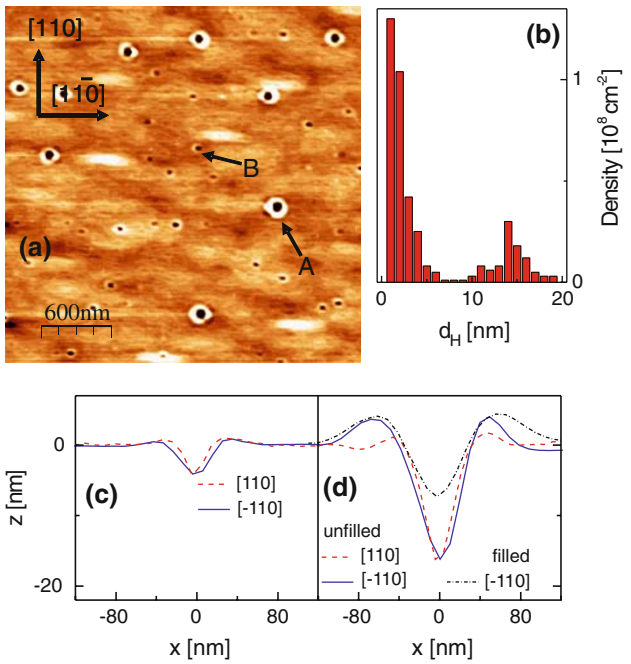

Fig. 2 **a** AFM image of an AlGaAs surface after Al LDE at $T_1 = T_2 = 620°$, $t_1 = 6$ s, $t_2 = 180$ s, and $F = 0.47$ ML/s. **b** Distribution of the hole depth d_H. **c** Profiles of the shallow hole marked by arrow "B" in Fig. 2a along [110] and [−110] azimuth. **d** Profiles of the deep hole marked by *arrow* "A" in Fig. 2a and of a typical deep hole after filling with $d_F = 0.57$ nm GaAs

process at higher temperatures. Due to decomposition of the surface, the maximum temperature for LDE on AlGaAs is about 630°. Therefore, for high-temperature fabrication of uniform QDs, the LDE process was performed on more stable AlAs surfaces (type II samples). For AFM characterization, this has the disadvantage that the highly reactive AlAs surface oxidizes very fast under air. Therefore, measurements of the nanohole profile were not possible on pure AlAs surfaces. From the AFM images, we determine the nanohole density to be 4×10^8 cm^{-2}. Furthermore, the size of the hole openings indicates that LDE holes on AlAs are shaped like the deep nanoholes on AlGaAs and that no shallow holes have been formed.

For the LDE QD fabrication, the nanoholes were filled with GaAs at a substrate temperature of 600° in a pulsed mode by applying several pulses with 0.5 s growth and 30 s pause, respectively. Finally, the QDs were capped by a 120-nm-thick AlGaAs barrier. A scheme of the resulting layer sequences for samples of type I and II is shown in Fig. 3. Figure 2d shows the AFM profile of a typical deep hole after filling with GaAs. The data demonstrate that pulsed-mode deposition of an only $d_f = 0.45$-nm-thin GaAs layer fills the nanohole to a height of about $h_{QD} = 7$ nm. In Ref. [21], this experimental filling level was explained quantitatively with a model in which the part of the GaAs flux impinging on the area of the nanohole opening migrates downwards and fills up the hole starting from its bottom. Very importantly, deep holes are only partially filled with a filling level defined by the precise layer thickness control of the MBE technique. This results for samples of type II in very uniform GaAs QDs. These QDs are shaped like inverted cones with slightly elliptical base area (aspect ratio 1 : 1.2) and height h_{QD} being perfectly controlled by the thickness d_f of the GaAs layer deposited for filling. On the other hand, flat holes in type I samples are completely filled and the height of these QDs reflect the very broad hole depth distribution.

Optical Properties of LDE QDs

Macro-photoluminescence (PL) measurements of QD ensembles were performed at $T = 3.5$ K and micro-PL measurements of single QDs at $T = 7$ K. Using macro-PL, a reference sample without filling shows no optical signal (Fig. 4a) and, thus, demonstrates that there is no background emission from the AlGaAs layers. A second reference sample with $d_f = 0.65$ nm but without etching shows one strong PL peak at $E = 1.900$ eV (Fig. 4b) that is related to the GaAs quantum well. Interestingly, a quantum well–related peak is missing or very weak for the samples containing LDE QDs. Probably, the excitons from the GaAs quantum well migrate into the energetically favorable QDs and recombine there. PL measurements of samples that contain QDs fabricated in type I samples show a broadband optical emission without pronounced peaks. Furthermore, no clear dependence on the GaAs filling level is visible. We attribute the broad PL emission to the

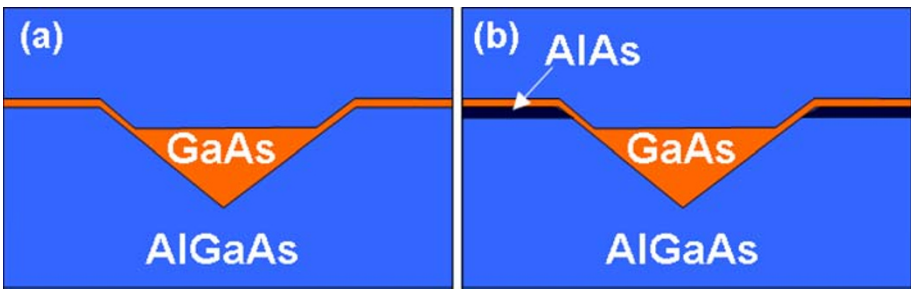

Fig. 3 Schematic cross-section through a deep nanohole **a** in a sample of type I and **b** in a type II sample with additional AlAs layer

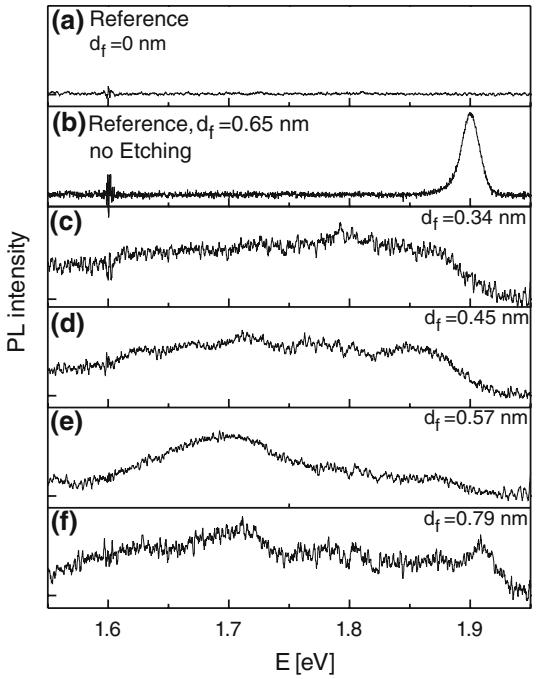

Fig. 4 PL measurements at $T = 3.5$ K of several type I samples. **a** Reference sample without filling, **b** reference sample without LDE step, **c–f** samples with LDE and filling where d_f was varied as indicated. The laser energy was 2.33 eV, and the excitation power $I_e = 450$ W/cm^2

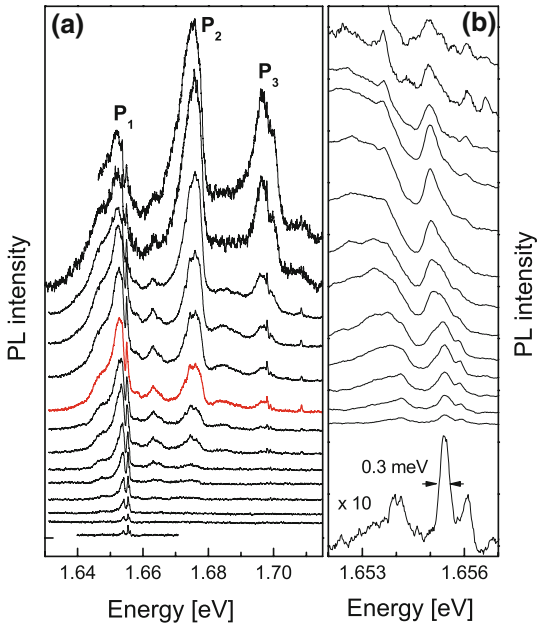

Fig. 5 **a** Micro-PL power series of a single type I GaAs QD from the sample of Fig. 4e with $d_f = 0.57$ nm. **b** Zoomed part of the spectra. The laser energy was 1.96 eV, and the excitation power I_e was varied from I_e 8 up to 1,700 W/cm^2. The *red* spectrum in (**a**) was measured using $I_e = 450$ W/cm^2, which is equal to the conditions applied in Fig. 4

nonuniform depth distribution of the completely filled shallow nanoholes.

Excitation power I_e dependent micro-PL spectra of a single QD in a type I sample with $d_F = 0.57$ nm are shown in Fig. 5. The QD was selected by focusing the exciting laser beam. Clearly visible at low excitation power are sharp excitonic lines and the occurrence of multiexcitonic features [29] at lower energy with increase of I_e (Fig. 5b). Furthermore, also excited states (peaks P_2 and P_3 in Fig. 5a) arise at higher I_e. From a comparison of the ground-state energy (peak P_1 in Fig. 5a) of around 1.65 eV with data shown in Ref. [21], we estimate a QD height of about 6 nm. The excited-state peak P_2 has a quantization energy of 20 meV and peak P_3 of 42 meV. According to Ref. [21], the peak P_2 might represent recombinations of ground-state electrons with holes in the second excited state and peak P_3 recombinations between electrons and holes from the first excited states. The spectrum plotted in red color in Fig. 5a was measured at an excitation power of $I_e = 450$ W/cm^2 which is equal to the conditions applied for the measurement of the macro-PL data shown in Fig. 4. Therefore, the broadband PL spectra shown in Fig. 4 are composed of a large number (about 10^4) of single dot spectra similar to that of Fig. 5a, but with respective emission energy being shifted due to the nonuniform QD size.

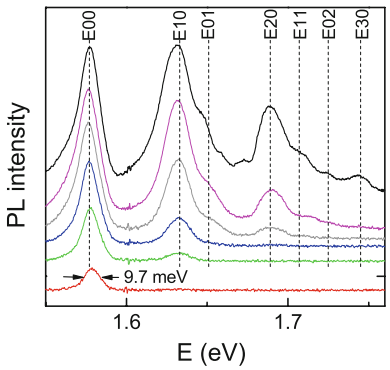

Fig. 6 PL measurements of type II LDE QDs with $h_Q = 7.6$ nm at varied excitation power $I_e = 8.5\ldots450$ W/cm^2. The laser energy was 2.33 eV. *Dashed lines* indicate calculated transition energies assuming a parabolic confinement potential

Figure 6 shows PL spectra from type II QDs fabricated at the higher temperature on AlAs surfaces. Importantly, at low I_e, ensembles of these QDs exhibit a very sharp PL line with minimum full width at half maximum as small as 9.7 meV. Here, only partially filled deep holes form highly uniform QDs. From the filling level $d_F = 0.57$ nm, we calculate a QD height of 7.6 nm according to Ref. [21]. Additional sharp peaks arise with increasing I_e that are related to excited states. For an understanding of the PL, spectra we approximate the electron and hole energy quantization due to the anisotropic lateral confinement with

two parabolic potentials along x and y direction. Optical recombinations between electrons and holes from states with identical quantization numbers n_x, n_y are denoted in the form $E_{n_x n_y} = E_{00} + n_x\hbar\omega_x + n_y\hbar\omega_y$, with the oscillator frequencies ω_x and ω_y. In Fig. 6 a, the PL data are compared with energy levels calculated using $E_{00} = 1.577$ eV, and equidistant quantization energies $\hbar\omega_x = 56$ meV and $\hbar\omega_y = 74$ meV. Our approach of a parabolic potential with a slightly anisotropic QD base describes the data very well. Measurements of the dependence of the QD optical emission on QD height are discussed in Ref. [21] and theoretical results considering a similar type of QDs in Ref. [30].

Conclusions

The local droplet etching of nanoholes in semiconductor surfaces represents a powerful new degree of freedom for the design of novel semiconductor heterostructures and devices. This method allows to tune the structural properties over a wide range by adjusting the materials and the process parameters. Self-assembled quantum dots are created by filling of nanoholes in AlGaAs with GaAs. Dependent on the sample design and the LDE process parameters, these QDs show either broadband optical emission or discrete sharp lines. Broadband light sources are very attractive because of their wide range of applications, which include fiber-optic gyroscopes, fiber-optic sensors, optical coherence tomography, and wavelength-division multiplexing transmission [31]. On the other hand, self-assembly of strain-free quantum dots with very uniform size distribution may help to overcome some limitations of the widely used Stranski–Krastanov InAs QDs.

Acknowledgments The authors would like to thank the "Deutsche Forschungsgemeinschaft" for financial support via SFB 508 and GrK 1286.

References

1. D. Bimberg, M. Grundmann, N.N. Ledentsov, *Quantum Dot Hetrostructures* (Wiley, Chichester, 1999)
2. G.T. Liu, A. Stintz, H. Li, K.J. Malloy, L.F. Lester, Electron. Lett. **35**, 1163 (1999)
3. E. Knill, R. Laflamme, G.J. Milburn, Nature **409**, 46 (2001)
4. P. Michler, A. Kiraz, C. Becher, W.V. Schoenfeld, P.M. Petroff, L. Zhang, E. Hu, A. Imamoglu, Science **290**, 2282 (2000)
5. C. Santori, M. Pelton, G. Solomon, Y. Dale, Y. Yamamoto, Phys. Rev. Lett. **86**, 1502 (2001)
6. J.M. Moison, F. Houzay, F. Barthe, L. Lepronce, E. Andre, O. Vatel, Appl. Phys. Lett. **64**, 196 (1994)
7. A. Madhukar, Q. Xie, P. Chen, A. Konkar, Appl. Phys. Lett. **64**, 2727 (1994)
8. D. Leonard, M. Krishnamurthy, S. Fafard, J.L. Merz, P.M. Petroff, J. Vac. Sci. Technol. B **12**, 1063 (1994)
9. D. Leonard, S. Fafard, Y.H. Zhang, J.L. Merz, P.M. Petroff, J. Vac. Sci. Technol. B **12**, 2516 (1994)
10. N. Koguchi, K. Ishige, Jpn. J. Appl. Phys. **32**, 2052 (1993)
11. M. Yamagiwa,T. Mano, T. Kuroda, T. Tateno, K. Sakoda, G. Kido, N. Koguchi, Appl. Phys. Lett. **89**, 113115 (2006)
12. S. Huang, Z. Niu, Z. Fang, H. Ni, Z. Gong, J. Xia, Appl. Phys. Lett. **89**, 031921 (2006)
13. Ch. Heyn, A. Stemmann, A. Schramm, H. Welsch, W. Hansen, Á. Nemcsics, Phys. Rev. B **76**, 075317 (2007)
14. T. Mano, K. Watanabe, S. Tsukamoto, H. Fujioka, M. Oshima, N. Koguchi, Jpn. J. Appl. Phys. **38**, L1009 (1999)
15. T. Mano, K. Watanabe, S. Tsukamoto, N. Koguchi, H. Fujioka, M. Oshima, C.D. Lee, J.Y. Leem, H.J. Lee, S.K. Noh, Appl. Phys. Lett. **76**, 3543 (2000)
16. J.S. Kim, N. Koguchi, Appl. Phys. Lett. **85**, 5893 (2004)
17. Ch. Heyn, A. Stemmann, A. Schramm, H. Welsch, W. Hansen, Á. Nemcsics, Appl. Phys. Lett. **90**, 203105 (2007)
18. Zh.M. Wang, B.L. Liang, K.A. Sablon, G.J. Salamo, Appl. Phys. Lett. **90**, 113120 (2007)
19. A. Stemmann, Ch. Heyn, T. Köppen, T. Kipp, W. Hansen, Appl. Phys. Lett. **93**, 123108 (2008)
20. Ch. Heyn, A. Stemmann, W. Hansen, J. Crystal Growth **311**, 1839 (2009)
21. Ch. Heyn, A. Stemmann, T. Köppen, Ch. Strelow, T. Kipp, S. Mendach, W. Hansen, Appl. Phys. Lett. **94**, 183113 (2009)
22. L.H. Lee, Z.M. Wang, M.E. Ware, K.C. Wijesundara, M. Garrido, E.A. Stinaff, G.J. Salamo, Cryst. Growth Des. **8**, 1945 (2008)
23. A.Z. Li, Z.M. Wang, J. Wu, Y, Xie, K.A. Sablon, G.J. Salamo, Cryst. Growth Des. **9**, 2941 (2009)
24. A. Stemmann, Ch. Heyn, W. Hansen, J. Appl. Phys. **106**, 064315, (2009)
25. C.Z. Tong, S.F Yoon, Nanotechnology **19**, 365604 (2008)
26. Ch. Heyn, A. Stemmann, R. Eiselt, W. Hansen, J. Appl. Phys. **105**, 054316 (2009)
27. Ch. Heyn, A. Stemmann, W. Hansen, Appl. Phys. Lett. **95**, 173110 (2009)
28. W. Ostwald, Z. Phys. Chem. **34**, 495 (1900)
29. A. Rastelli, S. Stufler, A. Schliwa, R. Songmuang, C. Manzano, G. Costantini, K. Kern, A. Zrenner, D. Bimberg, O.G. Schmidt, Phys. Rev. Lett. **92**, 166104 (2004)
30. Shu-Shen Li, Kai Chang, Jian-Bai Xia, Phys. Rev. B **71**, 155301 (2005)
31. C.Y. Ngo, S.F. Yoon, S.J. Chua, in *Quantum Dots: Research, Technology and Applications*, ed. by R.W. Knoss (Nova Science Publishers, New York, 2008), pp. 203–242